Resonances in rotationally inelastic scattering of NH_3 and ND_3 with H_2

Qianli Ma (马千里),[1,a)] Ad van der Avoird,[2,b)] Jérôme Loreau,[3] Millard H. Alexander,[4,c)] Sebastiaan Y. T. van de Meerakker,[2] and Paul J. Dagdigian[1,d)]
[1]*Department of Chemistry, The Johns Hopkins University, Baltimore, Maryland 21218-2685, USA*
[2]*Institute for Molecules and Materials, Radboud University, Heyendaalseweg 135, 6525 AJ Nijmegen, The Netherlands*
[3]*Service de Chimie Quantique et Photophysique C. P. 160/09, Université Libre de Bruxelles (ULB), 50 Ave. F. D. Roosevelt, 1050 Brussels, Belgium*
[4]*Department of Chemistry and Biochemistry and Institute for Physical Science and Technology, University of Maryland, College Park, Maryland 20742-2021, USA*

(Received 29 May 2015; accepted 8 July 2015; published online 28 July 2015)

We present theoretical studies on the scattering resonances in rotationally inelastic collisions of NH_3 and ND_3 molecules with H_2 molecules. We use the quantum close-coupling method to compute state-to-state integral and differential cross sections for the NH_3/ND_3–H_2 system for collision energies between 5 and 70 cm^{-1}, using a previously reported potential energy surface [Maret *et al.*, Mon. Not. R. Astron. Soc. **399**, 425 (2009)]. We identify the resonances as shape or Feshbach resonances. To analyze these, we use an adiabatic bender model, as well as examination at the scattering wave functions and lifetimes. The strength and width of the resonance peaks suggest that they could be observed in a crossed molecular beam experiment involving a Stark-decelerated NH_3 beam. © *2015 AIP Publishing LLC.* [http://dx.doi.org/10.1063/1.4927074]

I. INTRODUCTION

Resonances are among the most intriguing phenomena in scattering experiments.[1–4] In inelastic scattering, a resonance corresponds to formation of a quasibound level during the collision[5,6] and usually manifests as structure in the energy dependence of cross sections.[1] We use the term "shape" resonance if the quasibound level correlates with the initial or final monomer levels of the colliding partners, or "Feshbach" resonance, if the quasibound level correlates with a monomer level energetically inaccessible ("closed") at the collision energy in question.[2]

An accurate potential energy surface (PES) is the foundation for the theoretical study of collision dynamics. Although bound van der Waals states of the two collision partners depend mainly upon the attractive part of the PES, quasibound levels will be sensitive also to the repulsive portion of the PES. Since the position and shape of scattering resonances is a distinctive fingerprint of the PES,[7,8] agreement with experiment gives confidence in the subsequent use of a PES in the prediction of rate coefficients and other kinetic quantities difficult or impossible to measure.

The observation of resonances in crossed molecular beam experiments requires low collision energy and high energy resolution, as well as high initial-state purity.[9–11] Scattering resonances have been observed in mostly atomic, elastic collisions[12–14] and in the reactive $F + HD \rightarrow HF + D$ system.[15] Recently, in a merged-beam geometry, shape (also called orbiting) resonances were seen in Penning ionization collisions of metastable helium atoms with argon atoms or H_2 molecules at collision energies as low as 0.01 K.[16,17] Both shape and Feshbach resonances were observed in rotationally inelastic atom-molecule and molecule-molecule collisions.[18–21] Chefdeville *et al.*[18–20] investigated the scattering of H_2 by CO and O_2, while Bergeat *et al.*[21] studied CO–He scattering. In these experiments, the authors used Even–Lavie pulsed valves[22] to cool the molecular beams. By crossing the two beams at a small angle, they were able to lower the collision energy down to 3.5 cm^{-1}.

For molecules with nearly degenerate pairs of levels (such as the Λ-doublets of OH and the inversion doublets of NH_3) and/or multiple nuclear spin symmetries, standard cooling techniques are insufficient to produce a beam with population restricted to a single level. For these molecules, Stark deceleration[23,24] allows the production of cold beams confined to a single state. Scanning the collision energy would then provide an ideal means to search for resonances. Inspired by this possibility, our groups have searched theoretically for scattering resonances in the OH–He/Ne and the NH_3–He systems in calculations based on state-of-the-art PESs.[10,11] Both these systems manifest significant shape and Feshbach resonances. The features are narrow, with widths of ∼1 cm^{-1}. This poses a significant challenge to experiment.

Rotationally inelastic scattering of NH_3/ND_3 with H_2 has received considerable interest, not least because of the astrophysical importance.[25–35] Earlier work has focused on collisions out of the ground rotational level of *ortho*-NH_3, which is not suitable for Stark selection. Strong resonance peaks do appear in the computed energy dependence of state-to-state cross sections (see Fig. 2 in Ref. 29). Inelastic collisions of ND_3 with H_2 were investigated experimentally and theoretically by

[a)]Present address: Institut für Theoretische Chemie, Universität Stuttgart, Pfaffenwaldring 55, D-70569 Stuttgart, Germany.
[b)]Electronic mail: A.vanderAvoird@theochem.ru.nl
[c)]Electronic mail: mha@umd.edu
[d)]Electronic mail: pjdagdigian@jhu.edu

Tkáč *et al.*,[31] with special attention for the hexapole-selected 11− state of ND_3 that is a candidate for Stark deceleration (see Sec. II for the notation of the rotational levels).

In the present work, we study in detail resonances in the state-to-state cross sections of NH_3 and ND_3 out of this 11− level, using the PES computed by Maret *et al.*[29] This PES has been employed in a few studies of collision dynamics.[29,30,36,37] We will show that this system has strong and broad resonance peaks along with relatively large state-to-state cross sections. In addition, these resonances are well suited for investigation with crossed molecular beams.

This paper is organized as follows: in Sec. II, we briefly present the theory for rotationally inelastic scattering between a symmetric top and a closed-shell ($^1\Sigma^+$) diatomic molecule and describe our scattering calculations. In Sec. III, we introduce the PESs used in our calculations. We describe in Sec. IV the scattering resonances, both shape and Feshbach, that we found. To analyze these, we use the adiabatic bender model[38,39] as well as examination of the scattering wave function.[11] A discussion in Sec. V concludes.

II. SCATTERING CALCULATIONS

We label the rotational levels of the NH_3 and ND_3 symmetric top molecules as $jk\pm$, where j is the total angular momentum of the molecule, k is the projection of j on the C_3 axis, and ± is the umbrella inversion symmetry.[40] The NH_3 and ND_3 molecules have, respectively, two (*para* and *ortho*) and three (E, A_1, and A_2) nuclear spin modifications that do not interconvert during inelastic scattering.[40,41] The *para* or E nuclear spin rotational levels include k-stacks with k not a multiple of three, in particular the 11− level which is the candidate for Stark deceleration. For reference, we show in Fig. 1 the lower rotational levels of *para*-NH_3 and ND_3 (E nuclear spin symmetry).

We refer the reader to several previous papers for the full quantum description of inelastic collisions between a symmetric top molecule and a diatomic molecule in a $^1\Sigma$ electronic state.[26–28,42] We approximate the inversion doublet wave functions of NH_3/ND_3 as even and odd combinations of the two rigid equilibrium structures multiplied by rigid rotor wave functions, namely, $|jkm\varepsilon\rangle = 2^{-1/2}[|jkm\rangle + \varepsilon|jk,-m\rangle]$.

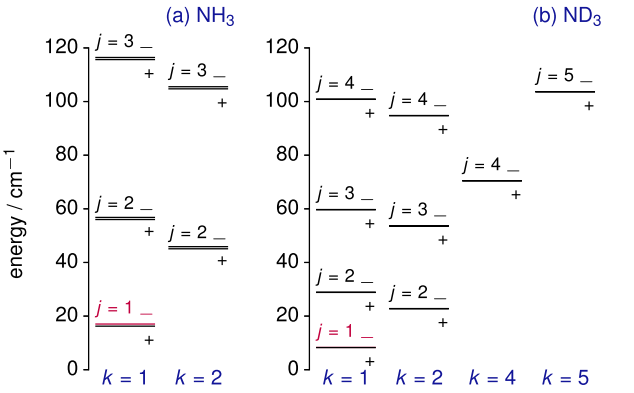

FIG. 1. Rotational level diagrams of (a) *para*-NH_3 and (b) ND_3 (E nuclear spin modification). The level 11− can be selected with a Stark decelerator and is labeled in red. The inversion doublets of ND_3 cannot be distinguished in the diagram due to the small inversion splitting.

The umbrella inversion symmetry is $-\varepsilon(-1)^j$. Previous investigations of inelastic scattering in the NH_3/ND_3–He and NH_3/ND_3–Ar systems[11,43,44] showed that this approximation gives excellent agreement with a more complete model based on full wave functions for the umbrella vibration–inversion.

Close-coupling calculations were performed both with the HIBRIDON suite of programs[45] and with a set of scattering programs developed in Nijmegen.[10,11,44,46] The availability of two totally distinct codes provided an ideal check of the accuracy and convergence of our calculations. We included in the close-coupling channel basis all *para* rotational levels of NH_3 with $j \le 6$ or E rotational levels of ND_3 with $j \le 7$. For collisions with *para*-H_2, the $j = 0$ and $j = 2$ levels of H_2 are included, while for *ortho*-H_2, only the $j = 1$ level. The maximum total angular momentum in the calculations was $J = 20$ for total energies <70 cm^{-1}. To determine the energy levels of isolated NH_3, we used rotational constants $B = 9.9402$ cm^{-1} and $C = 6.3044$ cm^{-1},[47] while for ND_3, we used $B = 5.1428$ cm^{-1} and $C = 3.1246$ cm^{-1}.[48] We assume an inversion splitting of 0.7903 and 0.053 cm^{-1} for NH_3 and ND_3, respectively, independent of j and k.[48–50] More details on the calculation of differential cross sections for molecule-molecule systems are contained in the supplementary material.[51]

III. POTENTIAL ENERGY SURFACES

To describe the NH_3–H_2 potential energy surface, we use the coordinate system defined in Fig. 2 of Ref. 28. The z axis lies along the three-fold symmetry axis of NH_3, and the Jacobian vector **R** that connects the centers of mass of the molecules has the polar angles (θ_1, ϕ_1). The orientation of the H_2 bond axis relative to this frame is defined by the angles (θ_2, ϕ_2). The interaction potential can be expanded either in Clebsch-Gordan coupled products of angular basis functions

$$V(R,\theta_1,\phi_1,\theta_2,\phi_2) = \sum_{l_1\mu_1 l_2 l} V_{l_1\mu_1 l_2 l}(R) \sum_{m_1} \langle l_1 m_1, l_2, -m_1 | l 0\rangle \times D^{l_1 *}_{m_1\mu_1}(0,-\theta_1,-\phi_1) \times D^{l_2 *}_{-m_1,0}(\phi_2,\theta_2,0) \quad (1)$$

or in an uncoupled product basis

$$V(R,\theta_1,\phi_1,\theta_2,\phi_2) = \sum_{l_1\mu_1 l_2 m_1} V_{l_1\mu_1 l_2 m_1}(R) D^{l_1 *}_{m_1\mu_1}(0,-\theta_1,-\phi_1) \times D^{l_2 *}_{-m_1,0}(\phi_2,\theta_2,0). \quad (2)$$

In the above equations, $V_{l_1\mu_1 l_2 l}$ and $V_{l_1\mu_1 l_2 m_1}$ are expansion coefficients, $\langle l_1 m_1, l_2, -m_1 | l 0\rangle$ is a Clebsch-Gordan coefficient, and $D^l_{m\mu}$ are rotation matrix elements.[52] The advantage of using the coupled expansion basis is that it is invariant under overall rotation of the system, so that the same expansion coefficients $V_{l_1\mu_1 l_2 l}$ can be used independently of the orientation of the frame in which the potential is expanded. Another frequently adopted angular expansion of the PES[53] uses a different set of angles to define the orientation of the molecules, but is in practice equivalent to Eq. (1).

We used the CCSD(T)/aug-cc-pVDZ PES with corrections from CCSD(T)/CBS calculations constructed by Maret *et al.*[29] We obtained from the authors the potential fitted by the

expansions of both Eqs. (1) and (2). We performed scattering calculations with both PESs. Because of the sensitivity of resonances to the underlying PES, the two expansions predict a slightly different resonance structure, as displayed in Fig. S1 of the supplementary material.[51] We recommend Eq. (1) for two reasons: (a) when similar terms in the two angular expansions are retained, the root mean square deviation (RMSD) is smaller [for example, at $R = 5$ bohr, the potential fitted to a 120-term expansion with Eq. (1) and a 167-term expansion with Eq. (2) has RMSD of 0.74 and 1.20 cm^{-1}, respectively] and (b) the evaluation of the potential matrix elements is easier.

To describe ND_3–H_2 collisions, the NH_3–H_2 PES needs to be modified to take into account the shift δ_{COM} of the center of mass. From the NH_3 geometry used in Ref. 29 ($r_{NH} = 1.9512\,a_0$ and $\angle_{HNH} = 107.38°$), we have $\delta_{COM} = 0.088\,530\,a_0$.

The *ab initio* NH_3–H_2 PES was determined on a grid of 29 values of R. At each value of R, 3000 orientations were used for the CCSD(T)/aug-cc-pVDZ PES but only 1000 for the CCSD(T)/CBS calculations. For ND_3–H_2, for each value of the NH_3–H_2 angle θ_1 (see Fig. 2 of Ref. 28), we introduce a corresponding θ_1' defined by trigonometry as

$$\theta_1' = \arccos \frac{R'^2 + \delta_{COM}^2 - R^2}{2\delta_{COM}R'}, \tag{3}$$

where R' is the intermolecular distance chosen to fit the ND_3–H_2 PES, and R is the corresponding intermolecular distance for NH_3–H_2 calculated from

$$R = -\delta_{COM}\cos\theta_1 + \sqrt{R'^2 - \delta_{COM}^2\sin^2\theta_1}. \tag{4}$$

We used these relations to transform the orientations $(\theta_1, \phi_1, \theta_2, \phi_2)$ for NH_3–H_2 to $(\theta_1', \phi_1, \theta_2, \phi_2)$ for ND_3–H_2 for each R' (from the same R grid used in the NH_3–H_2 calculations) and estimated the interaction energy for that geometry by splining the R dependence of the NH_3–H_2 interaction energies (*ab initio* points from Ref. 29) at this orientation. We then fit the ND_3–H_2 interaction energies with Eq. (1) and applied the long-range extrapolation using the method described in Ref. 29.

Figure 2 shows a comparison of R-dependence of the larger angular expansion coefficients for the NH_3 and ND_3 PESs. We see that the two PESs are quite similar, with three of the five larger expansion coefficients virtually identical and the other two showing only slight differences. This is not unreasonable given the small shift in the COM. The two expansion coefficients showing differences have significant contributions from multipole-multipole electrostatic interactions, with V_{1023} associated with the NH_3/ND_3-dipole–H_2-quadrupole interaction and V_{2024} with the quadrupole-quadrupole interaction.[54]

IV. RESULTS AND DISCUSSION

A. Collisions between NH_3 and *para*-H_2

1. Overview of the resonances

We show in Fig. 3 the energy dependence of the state-to-state integral cross sections for transitions from the 11− initial level at collision energies below 70 cm^{-1}. Below the threshold for rotational excitation, transition between the inversion doublets (11− → 11+) is the only inelastic process allowed. We observe rich resonance structure, with both broad and sharp peaks. Because of the deep well of the NH_3–H_2 PES [$D_e = 267$ cm^{-1} (Ref. 29)], we do not observe distinct groups of resonances associated with the opening of a particular channel, as are seen in molecule–rare gas systems.[10,11] We will show in Sec. IV A 2 that the resonances seen in Fig. 3 are Feshbach resonances. The broad peaks, a few wavenumbers in width and intensity more than three times the background inelastic cross sections, are particularly promising prospects for observation in a crossed beam experiment.

The 11− → 21+ transition also shows several resonances with magnitudes twice that of the background cross section. The analysis in Sec. IV A 3 reveals that these are shape resonances corresponding to quasibound states associated with the 21+ final level. Similar to the 11− → 21+ transition, the cross section for the 11− → 21− transition also displays a few shape resonances at similar collision energies, though smaller in magnitude. The resonances in the 11− → 22± transitions have contributions from both shape resonances, and Feshbach

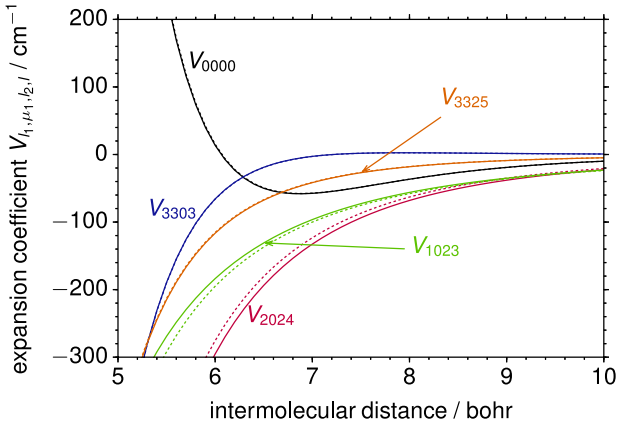

FIG. 2. Comparison between the larger expansion coefficients $V_{l_1\mu_1 l_2 l}$ [as defined in Eq. (1), only terms with non-negative μ_1 plotted due to symmetry properties discussed in Ref. 42] as a function of intermolecular distance, R, of the NH_3–H_2 PES described in Ref. 28 (dotted lines) and the ND_3–H_2 PES described in the present work (solid lines).

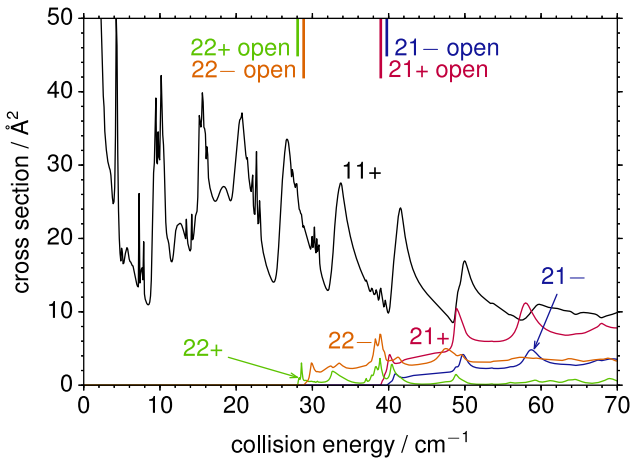

FIG. 3. State-to-state integral cross section as a function of collision energy for transition from the 11− level of *para*-NH_3 in collisions with *para*-H_2 in the $j = 0$ level. The curves are labelled by the final rotational level.

resonances caused by the quasibound states associated with the 21± levels.

The relative magnitudes of the state-to-state cross sections are significantly different for the NH_3–H_2 and NH_3–He systems. In particular, the transition to the 21+ level is much stronger when the collision partner is H_2. This can partly be explained with the differing anisotropies of the PESs. In collisions of NH_3 with $H_2(j = 0)$, the V_{1001} and V_{3003} terms directly couple the 11− and 21+ levels, while the V_{2002} term directly couples the 11− and 21− levels. These three coefficients in the NH_3–H_2 PES are comparable in magnitude at moderate to large intermolecular distances. For the NH_3–He PES, the corresponding V_{10} and V_{30} terms have significantly smaller magnitudes than the V_{20} term (see Fig. 3 of Ref. 11), giving rise to smaller 11− → 21+ cross sections. Further, with $H_2(j = 2)$ in the close-coupling channel basis, expansion terms with $l_2 > 0$ can affect the cross sections. These correspond physically to the interactions involving the quadrupole moment of H_2, which is obviously not present for the interaction of NH_3 with a spherical target.

2. Feshbach resonances in the 11− → 11+ transition

To understand the resonances in the 11− → 11+ transition, we plot in Fig. 4 the contributions to the integral cross section (partial cross sections) from each partial wave, distinguished by the total angular momentum J and the parity of the scattering wave functions under inversion. We observe several series of resonance structures consisting of peaks of similar shape. These peaks shift to higher collision energies as J increases. We expect that peaks within a given series are resonances arising from quasibound states associated with the same rotational level of NH_3. As J increases, the corresponding orbital angular momentum L increases, which leads to a higher centrifugal barrier and a higher quasibound state energy.

To investigate the origin of the resonances, we performed an adiabatic bender analysis similar to that described in Sec. IV C of Ref. 10. Here, we diagonalize the Hamiltonian exclusive of the radial kinetic energy for a given partial wave to obtain adiabatic bender curves. The energies of the van der Waals stretch levels supported by those curves are computed using a discrete variable representation (DVR) method.[55,56]

We display the derived adiabatic bender curves and quasibound level energies for the $J = 6$, + parity partial wave in Fig. 5 as an example. We see that the stretch levels supported by the adiabatic bender curves associated with the NH_3 22± levels, with energies 8.30, 15.71, and 22.30 cm^{-1} (red vertical lines in Fig. 4), are in reasonable agreement with the positions of the sharp resonance peaks that appear on the energy dependence of partial cross sections for this partial wave (the upper solid green curve in Fig. 4). The two lower stretch levels associated with the NH_3 21± levels, with energies 19.49 and 26.44 cm^{-1} (blue vertical lines in Fig. 4), agree with the positions of the broad resonance peaks. These results suggest that both the sharp and broad resonance peaks shown in Fig. 4 are Feshbach resonances, with the sharp peaks originating from quasibound states associated with the NH_3 22± level and the broad peaks from the 21± level.

One of the adiabatic bender curves in Fig. 5 has a bound stretch level at 33.18 cm^{-1}, at which no resonance appears in Fig. 4. A close look reveals that this adiabatic bender curve has avoided crossings with other curves, including those associated with a different NH_3 level. This is an example of the limitations of the adiabatic bender model. Near an avoided

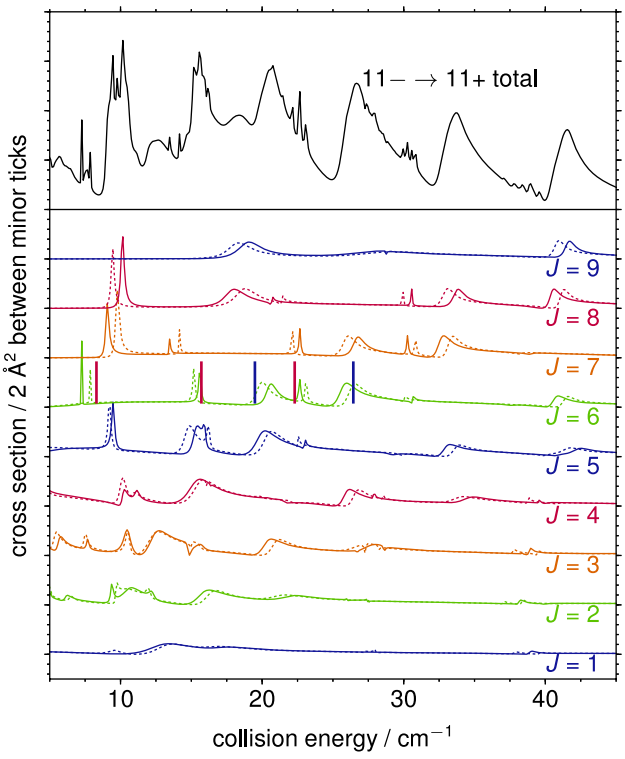

FIG. 4. Partial cross sections as a function of collision energy for the 11− → 11+ transition of *para*-NH_3 in collisions with *para*-H_2 in the $j = 0$ level. Solid lines represent the cross sections for + parity and dotted lines − parity for the given total angular momentum J. The red and blue vertical lines on the $J = 6$, + parity partial cross sections show the stretch level energies of the adiabatic bender curves (shown in Fig. 5) associated to the 22± and 11± levels of NH_3, respectively.

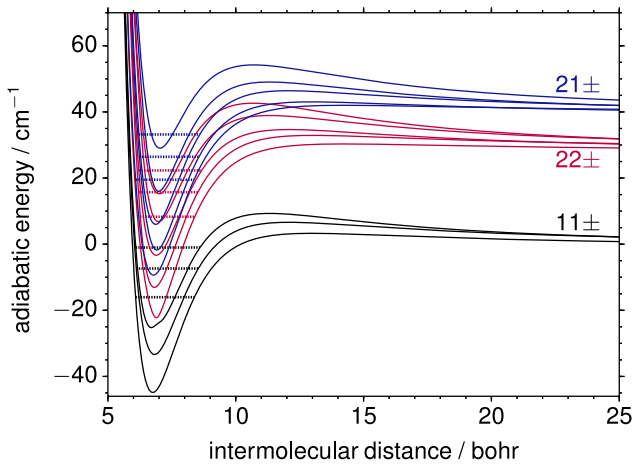

FIG. 5. Adiabatic bender curves for the interaction between *para*-NH_3 and *para*-H_2 for the $J = 6$, + parity partial wave. The colors of the lines indicate the asymptotic inversion doublet associated with the curves (the assignment is only approximate due to avoided crossings between curves). Quasibound states are shown as dotted horizontal lines. The zero of energy is the asymptotic energy of the 11− level of NH_3 and the $j = 0$ level of H_2.

crossing, the scattering wave function would change dramatically, and the separation of radial and angular functions, as assumed in the adiabatic bender model, would no longer be a good approximation. Such a phenomenon is analogous to nonadiabatic effects[57] in electronic structure theory. As shown in Fig. 5, the NH_3–H_2 adiabatic bender curves have well depths comparable or greater than the rotational level separation, and the adiabatic bender analysis is particularly vulnerable to these avoided crossings.

An alternative method of studying the (shape or Feshbach) resonances is to examine the contributions to the radial scattering wave functions from different channels that correspond to various monomer rotational levels and partial wave quantum numbers L.[11] The Nijmegen scattering program uses a renormalized Numerov propagator and it is relatively easy to generate these radial scattering wave functions. We plot in Fig. 6 such contributions to the squared scattering wave function of the $J = 6$, + parity partial wave at two collision energies. The two energies considered in Fig. 6 are close to each other, but the scattering wave functions are quite different. Figure 6(a) corresponds to a collision energy of 20.65 cm^{-1} where a broad resonance peak occurs. We see clearly that the 21− channel with $L = 4$ has a dominating amplitude in the region of the van der Waals well, but vanishes at larger R because this channel is still closed at this collision energy. This shows that the broad resonance peak around this energy corresponds to a Feshbach resonance associated with the 21− level of NH_3 and $L = 4$. Figure 6(b) represents a collision energy of 22.65 cm^{-1} at which there is a sharp resonance peak. The major contributor to the scattering wave functions here is the 22+ channel with $L = 6$, asymptotically closed at this collision energy. Hence, this sharp peak also corresponds to a Feshbach resonance, but involves the 22+ level of NH_3. For comparison, we also plotted the scattering wave functions at some nearby, off-resonance energies, but these plots only show the continuum functions of the channels open at the given collision energy and no channels with particularly large amplitudes in the region of the van der Waals well.

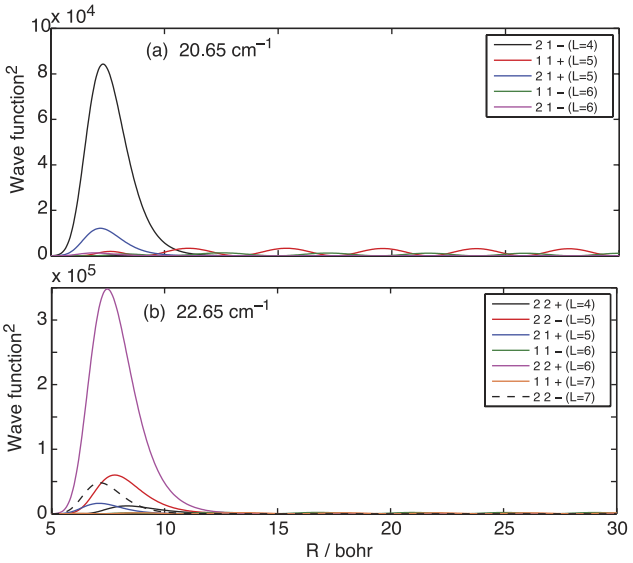

FIG. 6. Contributions of various rotational levels $jk\pm$ of NH_3 and partial waves L to the square of the scattering wave function with $J = 6$, + parity for the scattering of NH_3 in the 11− initial state and *para*-H_2 ($j = 0$). Collision energies are (a) 20.65 cm^{-1} and (b) 22.65 cm^{-1}.

TABLE I. Resonance peaks in state-to-state cross sections and corresponding quasibound states giving rise to the resonances in the 11− → 11+ transition of NH_3 in collisions with *para*-H_2 ($j = 0$). The associated NH_3 rotational levels $jk\pm$ and partial wave quantum numbers L are obtained from the wave function analysis described in Sec. IV A 2.

J	Parity	Energy / cm^{-1}	$jk\pm$ (L)
5	(+)	20.20	21+(4), 21−(3)
5	(−)	20.65	21−(4), 21+(3)
6	(+)	20.00	21+(4), 21−(5)
6	(−)	20.65	21−(4), 21+(5)
6	(−)	25.95	21+(5), 21−(4)
6	(+)	26.55	21−(5), 21+(4)
7	(−)	26.10	21+(5), 21−(6)
7	(+)	26.80	21−(5), 21+(6)
7	(+)	32.85	21+(6), 21−(5)
7	(−)	33.50	21−(6), 21+(5)
8	(+)	33.10	21+(6), 21−(7)
8	(−)	33.85	21−(6), 21+(7)
8	(−)	40.60	21+(7), 21−(6)
8	(+)	41.35	21−(7), 21+(6)
9	(−)	40.95	21+(7), 21−(8)
9	(+)	41.70	21−(7), 21+(8)
6	(+)	15.20	22+(5), 22−(6,4)
6	(−)	15.60	22−(5), 22+(6,4)
6	(−)	22.65	22+(6), 22−(5,7)
6	(+)	23.10	22−(6), 22+(7,5)
7	(−)	22.15	22+(6), 22−(7,5)
7	(+)	22.70	22−(6), 22+(7,5)
7	(+)	30.25	22+(7), 22−(6,8)
7	(−)	30.85	22−(7), 22+(8,6)
8	(+)	29.95	22+(7), 22−(8,6)
8	(−)	30.55	22−(7), 22+(8,6)

An overview of the resonances in the 11− → 11+ transition is given in Table I. One series of Feshbach resonances involves the 21± levels of NH_3, just like the $L = 4$ resonance illustrated in Fig. 6(a), with partial wave quantum numbers $L = 4$, 5, 6, and 7. The second series, illustrated for $L = 6$ in Fig. 6(b), involves the 22± levels of NH_3 with $L = 5$, 6, and 7. Figure 3 shows that resonances in the first series are all broad, while those in the second series are all sharp. This is related to which terms in the expansion of the potential couple these closed states to the open 11± states; for the 21± levels in the first series, these are primarily the $V_{l_1\mu_1 l_2 l}$ terms with $l_1 = 1$, 2, and 3 and $\mu_1 = 0$, while for the 22± levels in the second series, these are primarily the terms with $l_1 = 3$ and $\mu_1 = 3$. The plot of the expansion coefficients in Fig. 2 shows that the latter terms are considerably smaller, which explains why the resonances in the second series are much sharper than those in the first series. This agrees with the observation that the 11− → 21± transitions have larger cross sections than the 11− → 22± transitions, despite a larger energy gap (see Fig. 3). From the energy spacings between the resonances and the assigned L values, one can deduce an effective end-over-end rotational constant of the quasi-bound NH_3-*para*-H_2 complex. Both series of resonances correspond to a rotational constant of about 0.6 cm^{-1}. This value, combined with the reduced mass

of the complex, yields an effective R value of about 7.5 a_0, which agrees with the R value corresponding to the maximum in the dominant component of the scattering wave functions in Fig. 6. Noticeably, this is somewhat larger than the equilibrium distance $R_e = 6.1\ a_0$.

We see that the two techniques for analyzing the resonances agree on the origin of the resonances. The scattering wave function analysis, while slightly more computationally demanding, does not suffer from avoided crossings in the adiabatic bender analysis.

Additional information on the resonances can be obtained by looking at the phase shifts in the scattering wave function. These phase shifts can be obtained from the eigenvalues of the scattering matrix.[1,58] The top panel (a) of Fig. 7 shows the sums of the phase shifts in all open channels for various total angular momenta J for collision energies up to 28.1 cm^{-1}, where the 22+ channel opens and a jump in the phase shift sum occurs. Since we consider both parities ±, there are two curves for each J. From scattering theory, it follows that when a resonance occurs, the phase shift sum rapidly increases by π as a function of the collision energy.[1,58] In Fig. 7(a), we see this happening at the collision energies where the Feshbach resonances are found in the elastic and inelastic cross sections. The derivative of the phase shifts with respect to the energy gives the lifetime of the collision complex.[1] These lifetimes are shown in Fig. 7(b). This figure illustrates that at the energies where resonances occur, we indeed get long-lived collision complexes. One can see that each pair of curves belonging to the same J and different parities ± shows similar peaks, shifted by about 0.8 cm^{-1}, which is the splitting between the ± umbrella inversion tunneling states in NH_3. By comparing this figure with Fig. 4, one observes that the narrower the resonance, the longer its lifetime.

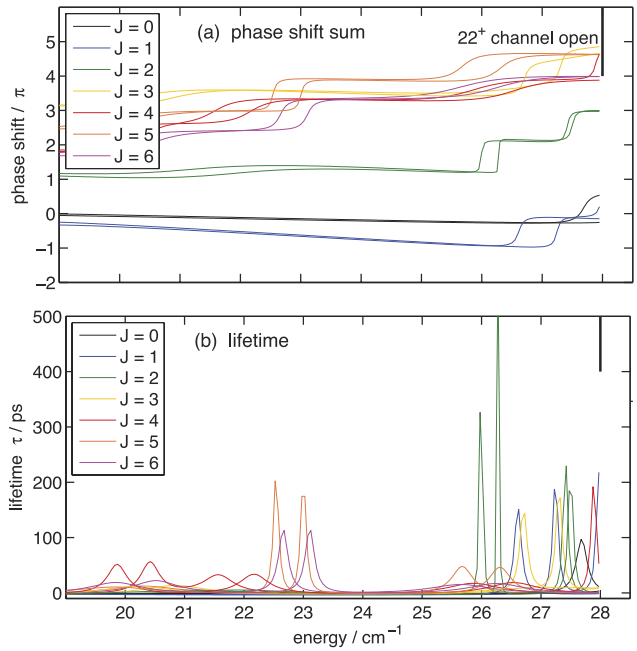

FIG. 7. (a) and (b) Phase shift sum and collision lifetime for different total angular momenta J for the scattering of NH_3 in the 11− initial state and *para*-H_2 ($j = 0$). The two curves drawn for each J value correspond to the ± parities of the overall scattering wave function.

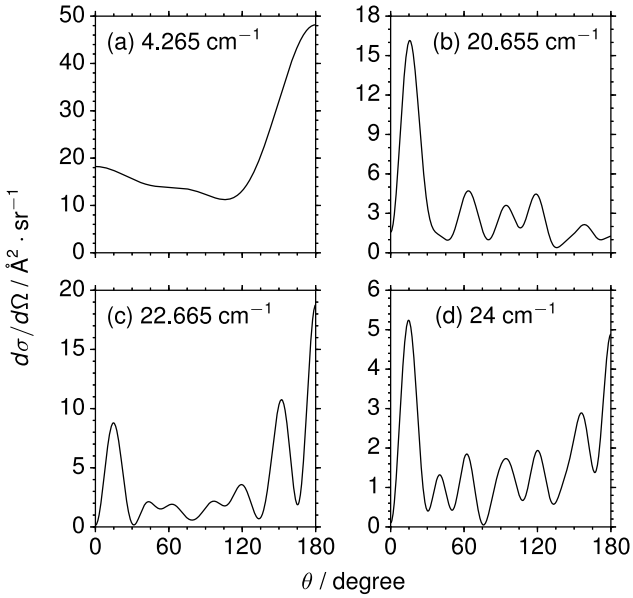

FIG. 8. Differential cross sections for the 11− → 11+ transition in NH_3 in collisions with *para*-H_2 $j = 0$ at several collision energies, labeled on each panel.

We also computed the differential cross sections (DCSs) at several resonance and off-resonance energies; these are shown in Fig. 8. The pattern of increased backward scattering at energies close to a resonance, as we found for the OH/NH_3–rare gas systems,[10,11] is less clear for NH_3–H_2 collisions. Figures 8(a) and 8(c) show DCSs at energies close to sharp resonance peaks, and we see significant backward scattering as expected. Backward scattering is even dominating at a collision energy of 4.265 cm^{-1}, corresponding to the first sharp resonance peak shown in Fig. 3. Figures 8(b) and 8(d) correspond to energies at a peak and a valley, respectively, among a series of broad resonance peaks. Surprisingly, we do not see strong backward scattering at the near-resonance energy. We note that the differential cross sections are not from the $J = 6$, + parity partial wave alone and there are significant contributions and interferences involving other partial waves.

3. Shape resonances in the 11− → 21+ transition

In this section, we analyze the resonance structure shown in the energy dependent 11− → 21+ cross section. Although not as dramatic as the resonances in the 11− → 11+ transition, the resonances in this transition have a relatively simple structure, and these moderately broad resonance peaks at slightly higher collision energies may facilitate the observation of resonances in molecular beam experiments.

We first show the partial cross sections for this transition in Fig. 9. We see the contribution to the resonance peaks is quite different from those shown in Fig. 4. Namely, each of the three peaks at collision energies of ≈40, 50, and 60 cm^{-1} has contributions from several partial waves. The three peaks have increasing widths as the energy increases. These are typical characteristics of a shape resonance.[10,59,60] This resonance structure, however, is distinguished from that observed in the NH_3–He and OH–He systems by the rapidly increasing background cross section and the large spacing between resonance

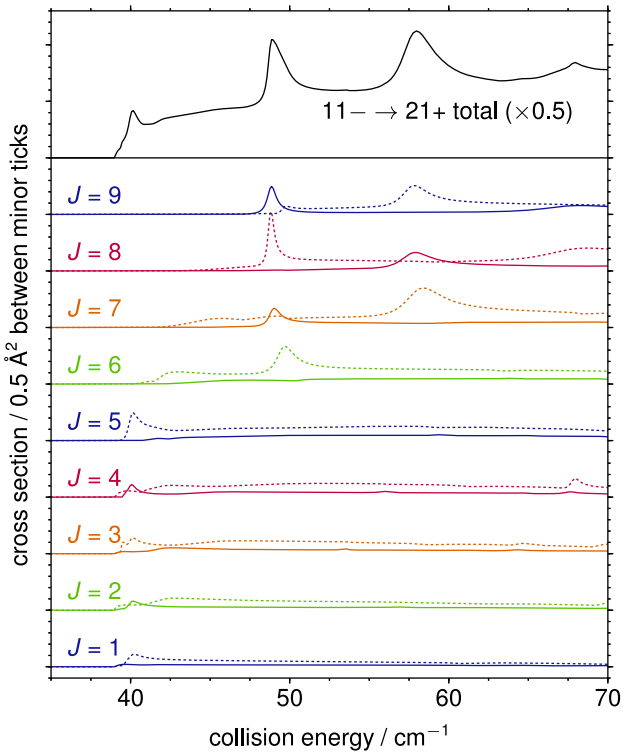

FIG. 9. Partial cross sections as a function of collision energy for the 11− → 21+ transition of *para*-NH_3 in collisions with *para*-H_2 in the $j = 0$ level. Solid lines represent the cross sections for + parity and dotted lines − parity for the given total angular momentum J.

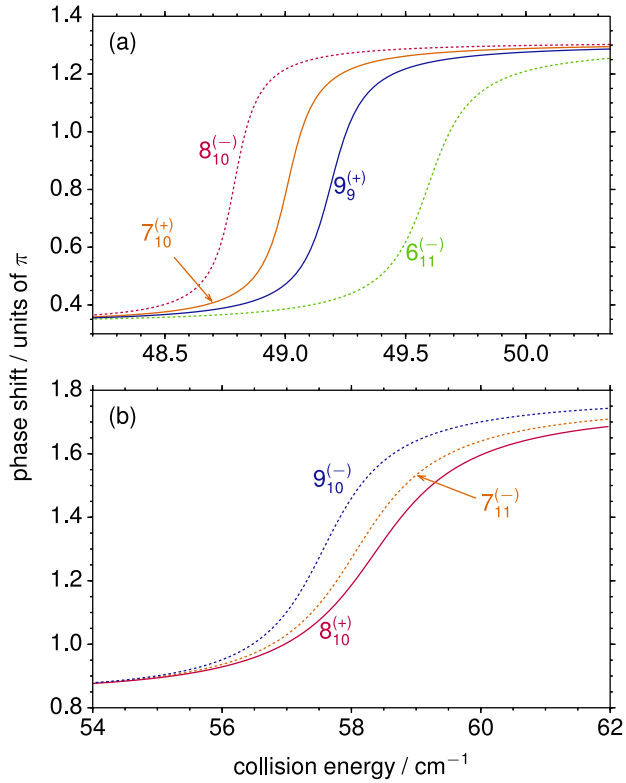

FIG. 10. Phase shifts as a function of collision energy for the collision between *para*-NH_3 and *para*-H_2, obtained from close coupling adiabatic bender curves that correlate asymptotically with NH_3 21+ and H_2 $j = 0$. The curves are labeled with $J_n^{(\pm)}$, where J, $(\pm)$, and n are the total angular momentum, the total parity of the scattering wave function, and the cardinal index, respectively. Only curves with $6 \le J \le 9$ that show a rapid increase of phase shift by π are plotted. The colors and line shapes of the curves match those for the corresponding partial waves in Fig. 9.

peaks. The large spacing is a direct consequence of the small reduced mass of the system and large centrifugal barriers.

To confirm the origin of these resonances, we again applied the adiabatic bender model used in Sec. IV A 2. The adiabatic bender curves look similar to those shown in Fig. 5 and are not shown here. After computing the adiabatic bender curves, we treat them as in a conventional one-dimensional scattering problem and compute the phase shift as a function of collision energy. We plot in Fig. 10 the phase shifts for all adiabatic bender curves associated with the 21+ level with $6 \le J \le 9$ that give rise to such changes in phase shift. We see clearly for each of the curves shown in Fig. 10 that the energy dependent partial cross section for the corresponding partial wave (Fig. 9) shows a resonance peak at a similar collision energy. Further, the widths of the resonances match those for a change of phase shift by π. This confirms that the resonances in the 11− → 21+ transition are shape resonances caused by quasibound states associated with the final level of the transition.

We note that there are four rotational levels below the 21+ level and the adiabatic bender curves related to that level have large cardinal indices. There are many avoided crossings between the adiabatic bender curves that make such phase shift analysis difficult and inaccurate. For this particular case, we found such analysis unsatisfactory.

The nature of these resonances was further confirmed by the scattering wave function analysis. It showed in this case that at the collision energies where the resonances occur, the wave functions in the van der Waals well are strongly dominated by contributions from specific channels, open at the given collision energy. This is the signature of a shape (or orbiting) resonance, and we could determine which rotational levels of NH_3 and which partial wave quantum numbers L mainly contribute to the corresponding quasi-bound states.

B. Collisions between NH_3 and *ortho*- and normal H_2

We show in Fig. 11 the collision energy dependence of the state-to-state cross sections out of the 11− level of NH_3 in collisions with *ortho*-H_2 in the $j = 1$ rotational level. We see that the 11− → 11+ transition dominates at the collision energies considered, and the cross section for this transition is considerably larger than the corresponding transition for collision with H_2 $j = 0$, displayed in Fig. 3. Unlike H_2 $j = 0$, the $j = 1$ level can polarize as it approaches the collision partner; the form of the $j = 1$ rotational wave function allows access to regions of the PES that are anisotropic in θ_2 (or $l_2 > 0$). Only $l_2 = 0$ terms in the angular expansion [see Eq. (1)] of the PES directly couple channels in collisions with H_2 $j = 0$, while many of the larger expansion coefficients have $l_2 > 0$. A similar enhancement in cross sections for collisions of *ortho*-H_2, as compared to those for *para*-H_2, has also been found in other molecule–H_2 inelastic collisions.[61,62]

We also see that the energy-dependent 11− → 11+ cross section plotted in Fig. 11 displays many overlapping resonances. This contrasts with the much smaller number of mostly

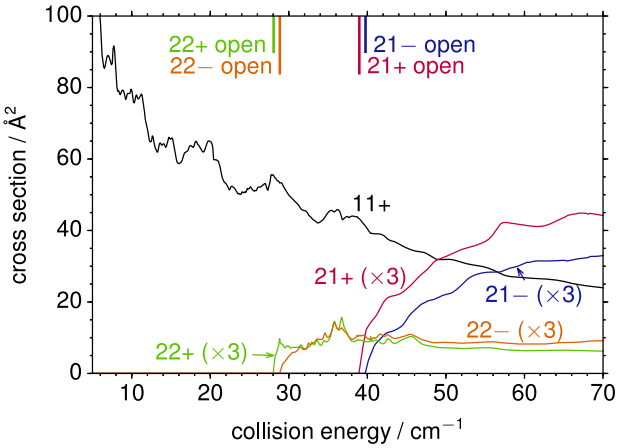

FIG. 11. State-to-state integral cross sections as a function of collision energy for transitions from the 11− level of *para*-NH_3 in collisions with *ortho*-H_2 in the $j = 1$ level. The final levels are indicated for each transition for which the cross section is plotted. The cross sections to the 21± and 22± levels are multiplied by 3 for clarity.

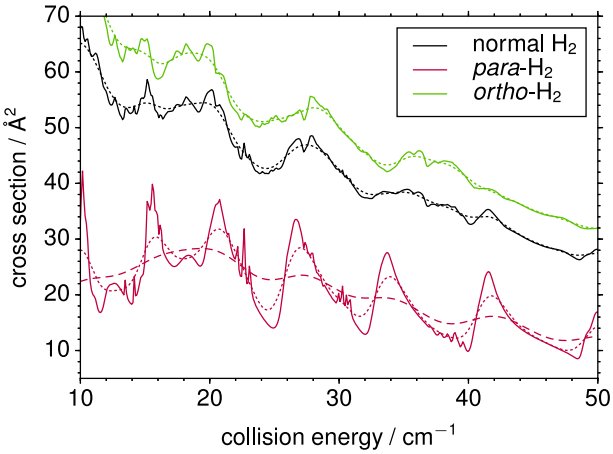

FIG. 12. Integral cross section as a function of collision energy for the 11− → 11+ transition of NH_3 in collisions with *para*-, *ortho*-, and normal (1:3 *para*:*ortho*) H_2. Computed cross sections (solid lines) and cross sections convoluted with Gaussian energy spread of FWHM of 2 cm^{-1} (dotted lines) and 5 cm^{-1} (dashed lines, only for NH_3–*para*-H_2) are plotted.

resolved resonances seen for collision of H_2 $j = 0$ (see Fig. 3). We also calculated the dissociation energy D_0 of the various nuclear spin species of NH_3–H_2, see Table II. The results in this table show that D_0 is considerably larger for NH_3–*ortho*-H_2($j = 1$) than for NH_3–*para*-H_2($j = 0$) since the effective PES for the former includes $l_2 > 0$ terms and the H_2 rotational wave function can polarize to sample the most attractive geometry of the complex. This is similar to other molecule–H_2 complexes in which the dissociation energy of the complex is significantly larger for *ortho*-H_2 than for *para*-H_2.[63–68] Thus, there are more bound, and quasi-bound, levels associated with NH_3–H_2($j = 1$) than with NH_3–H_2($j = 0$), and the resonance structure in the cross section for the 11− → 11+ transition is much more complicated for collision with H_2 $j = 1$ than for $j = 0$. We have not carried out a detailed analysis of the resonances seen in Fig. 11.

The shape resonances in the cross sections for the 11− → 21± transitions in collisions with H_2 $j = 1$ are small in magnitude relative to the non-resonant background, as compared to those when H_2 $j = 0$ is the collision partner. For the 11− → 22± transitions, the shape and Feshbach resonances associated with the 21± levels overlap and are small in magnitude (see Fig. 11). We expect that the resonances in these transitions will be difficult to observe in crossed beam experiments.

Normal hydrogen has an *ortho* to *para* ratio of 3:1. We plot in Fig. 12 the cross section for the NH_3 11− → 11+ transition in collision with *para*-, *ortho*-, and normal H_2. Because of the larger nuclear spin statistical weight and the larger cross section, the resonance structures for NH_3–normal H_2 (black lines in Fig. 12) are almost the same as for NH_3–*ortho*-H_2 (green lines in Fig. 12).

To estimate the feasibility of observing these resonances in molecular beam experiments, we also plot in Fig. 12 the cross sections for the 11− → 11+ transition of NH_3 in collisions with *para*-, *ortho*-, and normal H_2, convoluted with Gaussian collision energy spreads of two different widths. We see that with a 2 cm^{-1} energy resolution, the sharp resonance peaks disappear, but the broad resonance peaks are still resolved. However, with an energy spread of 5 cm^{-1}, only relatively weak oscillatory structures corresponding to the broad resonance peaks are left. Such structures would be difficult to observe in experiments. The best prospect for observing resonances in NH_3–H_2 collisions is with *para*-H_2.

TABLE II. Dissociation energies D_0 of the various nuclear spin species of NH_3–H_2.

NH_3–H_2	D_0 / cm^{-1}
ortho–para	32.43
para–para	34.25
ortho–ortho	59.78
para–ortho	66.00

C. Collisions between ND_3 and H_2

The ND_3 molecule has a smaller inversion splitting and is easier to manipulate with a Stark decelerator. Accordingly, we

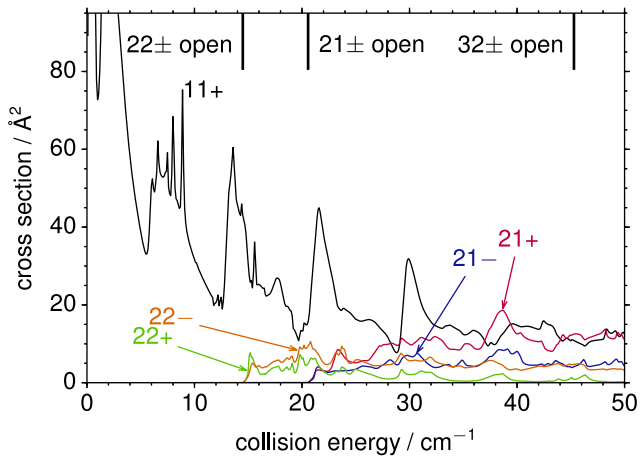

FIG. 13. State-to-state integral cross sections as a function of collision energy for transitions from the 11− level of ND_3 in collisions with *para*-H_2 ($j = 0$). The final levels are indicated for each transition for which the cross section is plotted.

investigate resonances in ND_3–H_2 collisions in this subsection. We present in Fig. 13 state-to-state integral cross sections as a function of collision energy for transitions from the 11− level of ND_3 in collisions with *para*-H_2 $j = 0$. There are pronounced resonance structures in the cross section for the 11− → 11+ transition. Similar to the NH_3–*para*-H_2 system, the broad peaks are Feshbach resonances associated with the 21± levels of ND_3, while the sharp peaks are Feshbach resonances associated with the 22± levels. While the NH_3–H_2 and ND_3–H_2 PESs are quite similar, the ND_3 rotational levels are more closely spaced. As a result, the ND_3 22± and 21± levels become open at lower collision energies; this in turn lowers the energies of the quasibound levels associated with these levels relative to the energy of the initial 11− level. It is therefore reasonable to see the resonance peaks appear at lower collision energies. Also, two higher inversion doublets, 32± and 31±, open at ≈45 and ≈51 cm^{-1}, respectively. Quasibound states associated with these levels also give rise to weaker resonance peaks in the plotted collision energy range, making the resonance structure more complicated.

The propensities for various transitions are generally the same for NH_3–H_2 and ND_3–H_2, consistent with the similarity of the PESs. However, the resonances in the 11− → 21± and 11− → 22± transitions of ND_3 show significant overlap and would be difficult to observe cleanly in crossed beam experiments. We do not show a detailed analysis of these resonances here.

V. CONCLUSIONS

We have presented calculations and analysis of resonances in rotationally inelastic scattering of NH_3 and ND_3, in the 11− initial level, with H_2 in $j = 0$ and $j = 1$. The large width of many resonances and relatively large resonance contributions to the cross sections, particularly *para*-H_2 collisions resulting in 11− → 11+ transitions, suggest that these resonances could be observed in molecular beam experiments. This would require resolution of the collision energy to better than ≈2 cm^{-1}, similar to what would be required for the OH–He/Ne and NH_3–He systems.[10,11] Notably, though, the NH_3–H_2 resonances are more prominent and the cross sections larger.

The required collision energy range could be achievable in Stark deceleration experiments in geometries where the beam crossing angle is less than 45°. The necessary energy resolution could be achieved by optimizing the kinematics of the experiment.[69] In the most elegant implementation, both integral and differential cross sections are recorded as a function of collision energy using the velocity map imaging detection.[70] The NH_3 molecule is particularly amenable to this combination of techniques, although the implementation of a recoil-free resonance-enhanced multi-photon ionization (REMPI) scheme can constitute a formidable challenge.[71] Experiments of this type are currently underway.

With the heavier D_2 as the collision partner, the resonance structures are more complex, with significant overlapping between resonances associated with different asymptotic rotational levels. The energy dependence of the cross sections is plotted in the supplementary material.[51] The reduced mass of NH_3–D_2 is almost twice that of NH_3–H_2. Thus, the zero-point energy of the deuterium complex will be smaller, so that the PES will support more bound and quasi-bound levels, including some levels with stretch quantum number greater than zero. Consequently, Feshbach resonances arising from quasi-bound levels associated with higher NH_3 rotational levels will appear at a lower energy and overlap significantly. In addition, the technique for *ortho* → *para* conversion is more efficient for H_2 compared to D_2. For all these reasons, then, D_2 is a less promising candidate for the study of resonances.

The ground rotational level (00+) of NH_3 is not amenable to Stark deceleration. Notwithstanding, we find that NH_3–H_2 cross sections for transitions from that level, particularly for the 00+ → 10+ transition, display interesting resonance structures with both broad and sharp resonance peaks. These energy-dependent cross sections are presented in the supplementary material.[51]

For any given system, the location and heights of resonances in inelastic scattering are a sensitive function of the underlying PES. The PES we used is that of Maret *et al.*,[29] based on *ab initio* calculations at the CCSD(T)/aug-cc-pVDZ level, corrected by similar CCSD(T) calculations with an aug-cc-pVTZ basis. To check the accuracy of the PES, for 3000 orientations at $R = 5\,a_0$, we have performed more sophisticated CCSD(T)-F12a calculations[72,73] with an aug-cc-pVTZ basis. We then fitted the interaction energy at these 3000 points using the same angular basis as used by Maret *et al.* We found that all ten expansion coefficients with the largest absolute values differ by less than 1% from those in this earlier PES. Therefore, we believe the PES of Maret *et al.* is sufficiently accurate for a careful study of the scattering resonance in this system.

ACKNOWLEDGMENTS

M.H.A. and P.J.D. acknowledge the support from the U.S. National Science Foundation (Grant No. CHE-1213322). S.Y.T.vdM. acknowledges financial support from the Foundation for Fundamental Research on Matter (FOM), which is financially supported by the Netherlands Organisation for Scientific Research (NWO) and by the European Research Council through a Starting Grant. J.L. thanks the FNRS and the Wiener-Anspach Foundation for the support. The authors are grateful to Claire Rist and to Alexandre Faure for providing the original data and the Fortran code for the NH_3–H_2 potential energy surface.

[1]M. S. Child, *Molecular Collision Theory* (Academic, London, New York, 1974).
[2]*Atom-Molecule Collision Theory: A Guide for the Experimentalist*, edited by R. B. Bernstein (Plenum, New York, 1979).
[3]J. Z. H. Zhang, *Theory and Application of Quantum Molecular Dynamics* (World Scientific Publishing Co. Pte. Ltd., 1999).
[4]S. Klaiman and I. Gilary, in *Unstable States in the Continuous Spectra II: Interpretation, Theory and Applications*, Advances in Quantum Chemistry Vol. 63, edited by E. B. Cleanthes, A. Nicolaides, and J. R. Sabin (Academic Press, 2012), Chap. 1, pp. 1–31.
[5]G. C. Schatz, Science **288**, 1599 (2000).
[6]P. Casavecchia and M. H. Alexander, Science **341**, 1076 (2013).
[7]D. W. Chandler, J. Chem. Phys. **132**, 110901 (2010).
[8]F. Lique, G. Li, H.-J. Werner, and M. H. Alexander, J. Chem. Phys. **134**, 231101 (2011).

[9]P. S. Żuchowski and J. M. Hutson, Phys. Rev. A **79**, 062708 (2009).
[10]K. B. Gubbels, Q. Ma, M. H. Alexander, P. J. Dagdigian, D. Tanis, G. C. Groenenboom, A. van der Avoird, and S. Y. T. van de Meerakker, J. Chem. Phys. **136**, 144308 (2012).
[11]K. B. Gubbels, S. Y. T. van de Meerakker, G. C. Groenenboom, G. Meijer, and A. van der Avoird, J. Chem. Phys. **136**, 074301 (2012).
[12]A. Schutte, D. Bassi, F. Tommasini, and G. Scoles, J. Chem. Phys. **62**, 600 (1975).
[13]A. Schutte, D. Bassi, F. Tommasini, and G. Scoles, Phys. Rev. Lett. **29**, 979 (1972).
[14]J. P. Toennies, W. Welz, and G. Wolf, J. Chem. Phys. **71**, 614 (1979).
[15]M. Qiu, Z. Ren, L. Che, D. Dai, S. A. Harich, X. Wang, X. Yang, C. Xu, D. Xie, M. Gustafsson, R. T. Skodje, Z. Sun, and D. H. Zhang, Science **311**, 1440 (2006).
[16]A. B. Henson, S. Gersten, Y. Shagam, J. Narevicius, and E. Narevicius, Science **338**, 234 (2012).
[17]E. Lavert-Ofir, Y. Shagam, A. B. Henson, S. Gersten, J. Kłos, P. S. Żuchowski, J. Narevicius, and E. Narevicius, Nat. Chem. **6**, 332 (2014).
[18]S. Chefdeville, T. Stoecklin, A. Bergeat, K. M. Hickson, C. Naulin, and M. Costes, Phys. Rev. Lett. **109**, 023201 (2012).
[19]S. Chefdeville, Y. Kalugina, S. Y. T. van de Meerakker, C. Naulin, F. Lique, and M. Costes, Science **341**, 1094 (2013).
[20]S. Chefdeville, T. Stoecklin, C. Naulin, P. Jankowski, K. Szalewicz, A. Faure, M. Costes, and A. Bergeat, Astrophys. J. Lett. **799**, L9 (2015).
[21]A. Bergeat, J. Onvlee, C. Naulin, A. van der Avoird, and M. Costes, Nat. Chem. **7**, 349 (2015).
[22]D. Pentlehner, R. Riechers, B. Dick, A. Slenczka, U. Even, N. Lavie, R. Brown, and K. Luria, Rev. Sci. Instrum. **80**, 043302 (2009).
[23]S. Y. T. van de Meerakker, H. L. Bethlem, and G. Meijer, Nat. Phys. **4**, 595 (2008).
[24]L. Scharfenberg, J. Kłos, P. J. Dagdigian, M. H. Alexander, G. Meijer, and S. Y. T. van de Meerakker, Phys. Chem. Chem. Phys. **12**, 10660 (2010).
[25]G. Danby, D. R. Flower, P. Valiron, P. Schilke, and C. M. Walmsley, Mon. Not. R. Astron. Soc. **235**, 229 (1988).
[26]A. Offer and D. R. Flower, J. Phys. B: At., Mol. Opt. Phys. **22**, L439 (1989).
[27]A. Offer and D. R. Flower, J. Chem. Soc., Faraday Trans. **86**, 1659 (1990).
[28]C. Rist, M. H. Alexander, and P. Valiron, J. Chem. Phys. **98**, 4662 (1993).
[29]S. Maret, A. Faure, E. Scifoni, and L. Wiesenfeld, Mon. Not. R. Astron. Soc. **399**, 425 (2009).
[30]L. Wiesenfeld, E. Scifoni, A. Faure, and E. Roueff, Mon. Not. R. Astron. Soc. **413**, 509 (2011).
[31]O. Tkáč, A. K. Saha, J. Loreau, Q. Ma, P. J. Dagdigian, D. H. Parker, A. van der Avoird, and A. J. Orr-Ewing, Mol. Phys. (published online).
[32]P. T. P. Ho and C. H. Townes, Annu. Rev. Astron. Astrophys. **21**, 239 (1983).
[33]D. R. Flower, Phys. Rep. **174**, 1 (1989).
[34]J. Lequeux and E. Roueff, Phys. Rep. **200**, 241 (1991).
[35]E. Roueff, D. C. Lis, F. F. S. van der Tak, M. Gerin, and P. F. Goldsmith, Astron. Astrophys. **438**, 585 (2005).
[36]F. Pirani, D. Cappelletti, L. Belpassi, and F. Tarantelli, J. Phys. Chem. A **117**, 12601 (2013).
[37]F. Daniel, A. Faure, L. Wiesenfeld, E. Roueff, D. C. Lis, and P. Hily-Blant, Mon. Not. Roy. Astron. Soc. **444**, 2544 (2014).
[38]S. L. Holmgren, M. Waldman, and W. Klemperer, J. Chem. Phys. **67**, 4414 (1977).
[39]M. H. Alexander, S. Gregurick, P. J. Dagdigian, G. W. Lemire, M. J. McQuaid, and R. C. Sausa, J. Chem. Phys. **101**, 4547 (1994).
[40]S. Green, J. Chem. Phys. **64**, 3463 (1976).
[41]O. Tkáč, A. J. Orr-Ewing, P. J. Dagdigian, M. H. Alexander, J. Onvlee, and A. van der Avoird, J. Chem. Phys. **140**, 134308 (2014).
[42]O. Tkáč, Q. Ma, C. A. Rusher, S. J. Greaves, A. J. Orr-Ewing, and P. J. Dagdigian, J. Chem. Phys. **140**, 204318 (2014).
[43]O. Tkáč, A. K. Saha, J. Onvlee, C.-H. Yang, G. Sarma, C. K. Bishwakarma, S. Y. T. van de Meerakker, A. van der Avoird, D. H. Parker, and A. J. Orr-Ewing, Phys. Chem. Chem. Phys. **16**, 477 (2014).
[44]O. Tkáč, A. K. Saha, J. Loreau, D. H. Parker, A. van der Avoird, and A. J. Orr-Ewing, J. Phys. Chem. A **119**, 5979 (2015).
[45]HIBRIDON is a package of programs for the time-independent quantum treatment of inelastic collisions and photodissociation written by M. H. Alexander, D. E. Manolopoulos, H.-J. Werner, B. Follmeg, P. J. Dagdigian, and others. More information and/or a copy of the code can be obtained from the website http://www2.chem.umd.edu/groups/alexander/hibridon.
[46]L. Scharfenberg, K. B. Gubbels, M. Kirste, G. C. Groenenboom, A. van der Avoird, G. Meijer, and S. Y. T. van de Meerakker, Eur. Phys. J. D **65**, 189 (2011).
[47]G. Danby, D. R. Flower, E. Kochanski, L. Kurdi, P. Valiron, and G. H. F. Diercksen, J. Phys. B: At. Mol. Phys. **19**, 2891 (1986).
[48]L. Fusina and S. N. Murzin, J. Mol. Spectrosc. **167**, 464 (1994).
[49]C. H. Townes and A. L. Schawlow, *Microwave Spectroscopy* (Dover, New York, 1975).
[50]C. Léonard, S. Carter, and N. C. Handy, Chem. Phys. Lett. **370**, 360 (2003).
[51]See supplementary material at http://dx.doi.org/10.1063/1.4927074 for the difference in the scattering resonances obtained with the two expansions of the PES, the explicit equation for computing differential cross sections for molecule-molecule collisions, and the energy-dependent state-to-state integral cross sections for collisions between *para*-NH_3 and D_2 and between *ortho*-NH_3 and H_2.
[52]R. N. Zare, *Angular Momentum: Understanding Spatial Aspects in Chemistry and Physics* (John Wiley & Sons, Inc., 1988).
[53]T. R. Phillips, S. Maluendes, A. D. McLean, and S. Green, J. Chem. Phys. **101**, 5824 (1994).
[54]C. G. Gray, Can. J. Phys. **54**, 505 (1976).
[55]D. T. Colbert and W. H. Miller, J. Chem. Phys. **96**, 1982 (1992).
[56]L. Tao and M. H. Alexander, J. Chem. Phys. **127**, 114301 (2007).
[57]D. R. Yarkony, in *Conical Intersections: Electronic Structure, Dynamics & Spectroscopy*, edited by W. Domcke, D. R. Yarkony, and H. Köppel (World Scientific Publishing Co. Pte. Ltd., 2004), Chap. 2, pp. 41–128.
[58]C. J. Ashton, M. S. Child, and J. M. Hutson, J. Chem. Phys. **78**, 4025 (1983).
[59]P. J. Dagdigian and M. H. Alexander, J. Chem. Phys. **130**, 164315 (2009).
[60]P. J. Dagdigian, A. Khachatrian, and V. I. Babushok, Appl. Opt. **49**, C58 (2010).
[61]K. Schreel and J. J. ter Meulen, J. Chem. Phys. **105**, 4522 (1996).
[62]A. Faure, N. Crimier, C. Ceccarelli, P. Valiron, L. Wiesenfeld, and M. L. Dubernet, Astron. Astrophys. **472**, 1029 (2007).
[63]C. M. Lovejoy, D. D. Nelson, and D. J. Nesbitt, J. Chem. Phys. **87**, 5621 (1987).
[64]D. C. Clary and P. J. Knowles, J. Chem. Phys. **93**, 6334 (1990).
[65]S. M. Miller, D. C. Clary, A. Kliesch, and H.-J. Werner, Mol. Phys. **83**, 405 (1994).
[66]X. Yang, E. Hwang, and P. J. Dagdigian, J. Chem. Phys. **104**, 8165 (1996).
[67]X. Tan, P. J. Dagdigian, and M. H. Alexander, Faraday Discuss. **118**, 387 (2001).
[68]A. van der Avoird and D. J. Nesbitt, J. Chem. Phys. **134**, 044314 (2011).
[69]L. Scharfenberg, S. Y. T. van de Meerakker, and G. Meijer, Phys. Chem. Chem. Phys. **13**, 8448 (2011).
[70]A. von Zastrow, J. Onvlee, S. N. Vogels, G. C. Groenenboom, A. van der Avoird, and S. Y. T. van de Meerakker, Nat. Chem. **6**, 216 (2014).
[71]J. Onvlee, S. N. Vogels, A. von Zastrow, D. H. Parker, and S. Y. T. van de Meerakker, Phys. Chem. Chem. Phys. **16**, 15768 (2014).
[72]T. B. Adler, G. Knizia, and H.-J. Werner, J. Chem. Phys. **127**, 221106 (2007).
[73]G. Knizia, T. B. Adler, and H.-J. Werner, J. Chem. Phys. **130**, 054104 (2009).